

# Anchoring and Upgrading Ultrafine NiPd on Room-Temperature-Synthesized Bifunctional NH<sub>2</sub>-N-rGO toward Low-Cost and Highly Efficient Catalysts for Selective Formic Acid Dehydrogenation

Jun-Min Yan, Si-Jia Li, Sha-Sha Yi, Ba-Ri Wulan, Wei-Tao Zheng, and Qing Jiang\*

Hydrogen is widely considered to be a sustainable and clean energy alternative to the use of fossil fuels in the future. Its high hydrogen content, nontoxicity, and liquid state at room temperature make formic acid a promising hydrogen carrier. Designing highly efficient and low-cost heterogeneous catalysts is a major challenge for realizing the practical application of formic acid in the fuel-cell-based hydrogen economy. Herein, a simple but effective and rapid strategy is proposed, which demonstrates the synthesis of NiPd bimetallic ultrafine particles (UPs) supported on NH<sub>2</sub>-functionalized and N-doped reduced graphene oxide (NH<sub>2</sub>-N-rGO) at room temperature. The introduction of the –NH<sub>2</sub>–N group to rGO is the key reason for the formation of the ultrafine and well-dispersed Ni<sub>0.4</sub>Pd<sub>0.6</sub> UPs (1.8 nm) with relatively large surface area and more active sites. Surprisingly, the as-prepared low-cost NiPd/NH<sub>2</sub>-N-rGO displays excellent hydrophilicity, 100% H<sub>2</sub> selectivity, 100% conversion, and remarkable catalytic activity (up to 954.3 mol H<sub>2</sub> (mol catalyst)<sup>–1</sup> h<sup>–1</sup>) for FA decomposition at room temperature even with no additive, which is much higher than that of the best catalysts so far reported.

Low-cost and efficient storage and release of hydrogen (H<sub>2</sub>) remain one of the most important challenges toward the fuel-cell-based hydrogen economy.<sup>[1]</sup> Formic acid (FA, HCOOH), a liquid at room temperature, is one of the major products of biomass processing, and has been identified as a safe and potential H<sub>2</sub> storage material due to its high hydrogen density (4.4 wt%), nontoxicity, and excellent stability.<sup>[2]</sup> To this end, FA should be selectively decomposed via dehydrogenation (HCOOH → CO<sub>2</sub> + H<sub>2</sub>) pathway (not follow dehydration route: HCOOH → CO + H<sub>2</sub>O), which is still heavily rely on noble metal of Pd,<sup>[3]</sup> and even so, the catalytic activity/selectivity is still far from satisfying even with the extra additives (HCOONa and/or triethylamine (NEt<sub>3</sub>)) and under elevated temperature (323–363 K).<sup>[4,5]</sup> To significantly improve the activity/selectivity and, especially,

lower the cost of the catalysts, it is urgent to introduce non-noble metals (NNMs), such as Co and Ni, to Pd to form the bimetallic NNM-Pd catalyst.<sup>[6]</sup> However, up to now, the activity/selectivity of NNM-containing (even <40 at% of NNMs) Pd-based catalysts is still very poor even at elevated temperature, especially without extra additives.<sup>[6]</sup> Thereafter, the development of facile and effective strategy to synthesize highly efficient catalysts with high content of NNMs is highly desirable while still very challenging for FA as a feasible H<sub>2</sub>-storage material.

In response, the fabrication of ultrafine particles (UPs) could increase the surface area and thus enhance the catalytic performances of NNM-containing Pd-based catalyst (NNM-Pd), while achieving good dispersity and avoiding the intrinsic aggregation of the UPs is still a big challenge, due to the absence of efficient catalyst support

that holds both large surface area and, especially, suitable interaction with the supported NNM-Pd UPs. Theoretically, N-doped graphene (N-graphene) could be employed as an ideal support, thanks to combined advantages of large surface area and enhanced adsorption ability for metal ions of metal precursors, which not only could in situ anchor the active metal nanoparticles, but also could offer more opportunity to tune the electronic structure of the particles (through the strong metal-to-support interaction (SMSI)) and thus enhance its catalytic activity.<sup>[7]</sup> Unfortunately, the hydrophobicity of pristine NNM-Pd/N-graphene nanocatalyst is not good to be applied in FA system due to the unavoidable aggregation and stacking in aqueous solution, which cannot ensure the ultrafine sizes and excellent dispersion of the NNM-Pd particles. In response, theoretically, the introduction of polar groups, such as –NH<sub>2</sub>, to N-graphene can endow the NNM-Pd/N-graphene with hydrophilicity, and the steric stabilization gained by –NH<sub>2</sub> groups may further suppress the aggregate of NNM-Pd UPs. Furthermore, the presence of –NH<sub>2</sub> alkaline groups has the priority to accelerate the cleavage of O–H bond in FA, which is the initial step of the FA dehydrogenation.<sup>[8]</sup> However, up to now, to the best of our knowledge, there is no report on NH<sub>2</sub>-functionalized N-graphene (NH<sub>2</sub>-N-graphene), to say nothing of being employed as a novel support for catalysts. Therefore, the

Prof. J.-M. Yan, S.-J. Li, S.-S. Yi, B.-R. Wulan,  
Prof. W.-T. Zheng, Prof. Q. Jiang  
Key Laboratory of Automobile Materials  
Ministry of Education  
Department of Materials Science and Engineering  
Jilin University  
Changchun 130022, China  
E-mail: jiangq@jlu.edu.cn

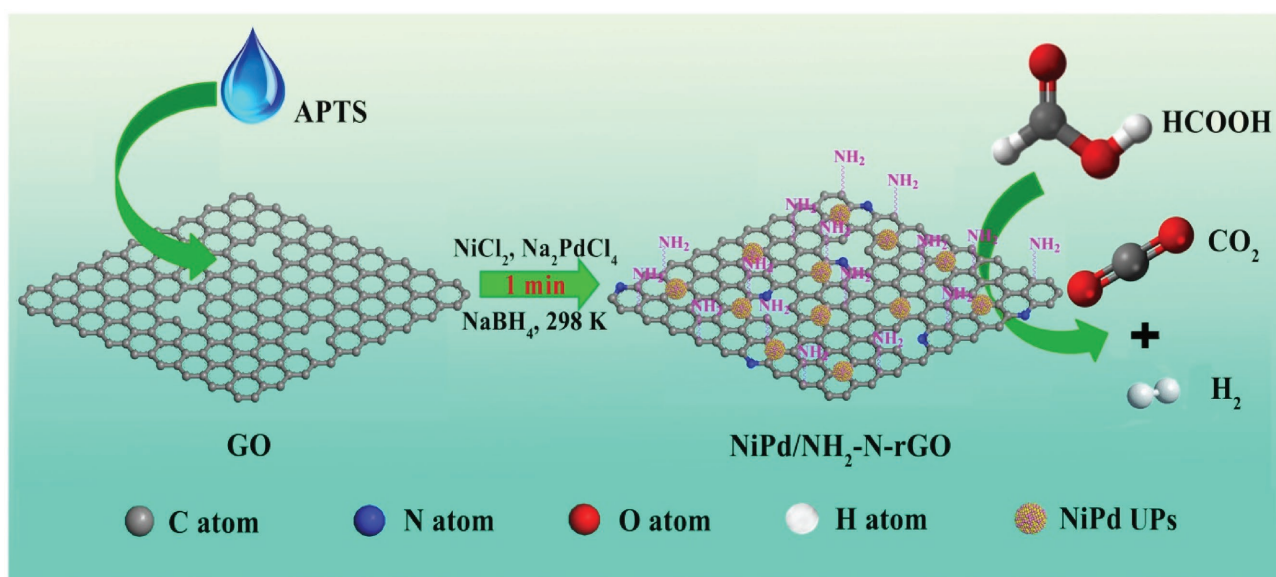
DOI: 10.1002/adma.201703038

development of a cost- and time-effective strategy to synthesize novel NH<sub>2</sub>-N-graphene-supported NNM-Pd UPs catalyst and then exploring its catalytic performances for decomposition of FA is highly desirable but very challenging.

Herein, we first propose and demonstrate a facile while effective and rapid strategy to synthesize well-dispersed NiPd bimetallic UPs (1.8 nm) anchored on the novel NH<sub>2</sub>-functionalized and N-doped reduced graphene oxide (NH<sub>2</sub>-N-rGO) at room temperature, wherein the metallic UPs and NH<sub>2</sub>-N-rGO are simultaneously one-step generated within 1 min, endowing the resultant NiPd/NH<sub>2</sub>-N-rGO catalyst with good hydrophilicity. Unexpectedly, when first used as novel catalyst for FA decomposition, the as-prepared low-cost NiPd/NH<sub>2</sub>-N-rGO shows 100% H<sub>2</sub> selectivity and excellent catalytic activity (up to 954.3 mol H<sub>2</sub> mol catalyst<sup>-1</sup> h<sup>-1</sup>) at room temperature even with no additive, which is much more higher than that of the best catalyst ever reported.

The design and fabrication processes of NiPd/NH<sub>2</sub>-N-rGO are illustrated in **Scheme 1**. Briefly, for the synthesis of Ni<sub>0.4</sub>Pd<sub>0.6</sub>/NH<sub>2</sub>-N-rGO,<sup>[9]</sup> the colorless (3-aminopropyl) triethoxysilane (APTS, 0.2 mL) is mixed with the previously prepared light brown and transparent GO aqueous solution by sonicating and stirring at 298 K to form the dark brown colloidal solution (Figure S1, Supporting Information), which indicates the strong interaction between APTS and GO.<sup>[10]</sup> And then aqueous solutions of NiCl<sub>2</sub> and Na<sub>2</sub>PdCl<sub>4</sub> (with Ni:Pd molar ratio of 0.4:0.6) are added to the above APTS-treated GO solution with magnetic stirring. Finally, NaBH<sub>4</sub> is dissolved into the above mixed solution, and the resultant black Ni<sub>0.4</sub>Pd<sub>0.6</sub>/NH<sub>2</sub>-N-rGO product can be rapidly obtained within 1 min. The product is separated and washed with water for the following characterization and catalytic FA dehydrogenation at 298 K without any additive. For comparison, Ni<sub>0.4</sub>Pd<sub>0.6</sub>/N-rGO and Ni<sub>0.4</sub>Pd<sub>0.6</sub>/rGO are also prepared.<sup>[9]</sup> Moreover, the molar ratio of Ni:Pd in NiPd/NH<sub>2</sub>-N-rGO system has been changed by several values (0:1, 0.2:0.8, 0.4:0.6, 0.6:0.4, 0.8:0.2, and 1:0).

**Figure 1** shows the transmission electron microscopy (TEM) images and the photographs of the as-prepared Ni<sub>0.4</sub>Pd<sub>0.6</sub>/NH<sub>2</sub>-N-rGO, Ni<sub>0.4</sub>Pd<sub>0.6</sub>/N-rGO and Ni<sub>0.4</sub>Pd<sub>0.6</sub>/rGO. Obviously, the Ni<sub>0.4</sub>Pd<sub>0.6</sub> UPs anchored on NH<sub>2</sub>-N-rGO (Figures 1a,d) demonstrate very good dispersity and very small particle size (≈1.80 nm; Figure S2a, Supporting Information). The accurate molar ratio of Ni:Pd in Ni<sub>0.4</sub>Pd<sub>0.6</sub>/NH<sub>2</sub>-N-rGO is determined to be about 0.43:0.57 by inductively coupled plasma-atomic emission spectrometry (ICP-AES), which agrees very well with the appointed value. The high-resolution TEM (HRTEM) image (Figure 1d, inset) reveals the crystalline nature of Ni<sub>0.4</sub>Pd<sub>0.6</sub> UPs, and the lattice spacing is measured to be 0.220 nm, which is between the (111) planes of face-centered cubic Ni (0.203 nm)<sup>[11]</sup> and Pd (0.224 nm).<sup>[12]</sup> On the other hand, Ni<sub>0.4</sub>Pd<sub>0.6</sub> nanoparticles supported on N-rGO without -NH<sub>2</sub> functionalization are also well dispersed (Figure 1b) but with the larger average size of ≈6.0 nm (Figure S2b, Supporting Information). However, Ni<sub>0.4</sub>Pd<sub>0.6</sub> on pure rGO is severely aggregated (Figure 1c), and the average particle size is ≈10.2 nm (Figure S2c, Supporting Information), which is larger than those supported on NH<sub>2</sub>-N-rGO and N-rGO. As expected, the prepared Ni<sub>0.4</sub>Pd<sub>0.6</sub>/NH<sub>2</sub>-N-rGO specimen demonstrates the excellent hydrophilicity, which does not sink in aqueous solution even after 40 h (Figure 1e). However, both Ni<sub>0.4</sub>Pd<sub>0.6</sub>/N-rGO and Ni<sub>0.4</sub>Pd<sub>0.6</sub>/rGO show the obvious phenomenon of sedimentation after only 20 min (Figure 1e). Based on the above TEM and sedimentation images, it can be reasonably believed that, after N doping, the resultant N-rGO has an effect to increase the dispersion of nanoparticles, and after further adding -NH<sub>2</sub> groups, the obtained NH<sub>2</sub>-N-rGO can make the catalyst to be hydrophilic and lead to the ultrafine sizes and excellent dispersion of UPs. Moreover, the Brunner–Emmet–Teller surface area for Ni<sub>0.4</sub>Pd<sub>0.6</sub>/NH<sub>2</sub>-N-rGO is measured to be 286.1 m<sup>2</sup> g<sup>-1</sup>, which is larger than that of Ni<sub>0.4</sub>Pd<sub>0.6</sub>/rGO (225.8 m<sup>2</sup> g<sup>-1</sup>); namely, the addition of -NH<sub>2</sub>-N groups on rGO is the key reason for the formation of the ultrafine and well-dispersed Ni<sub>0.4</sub>Pd<sub>0.6</sub> UPs with relatively large surface



**Scheme 1.** Schematic representation of the rapid preparation process of the NiPd/NH<sub>2</sub>-N-rGO catalyst.

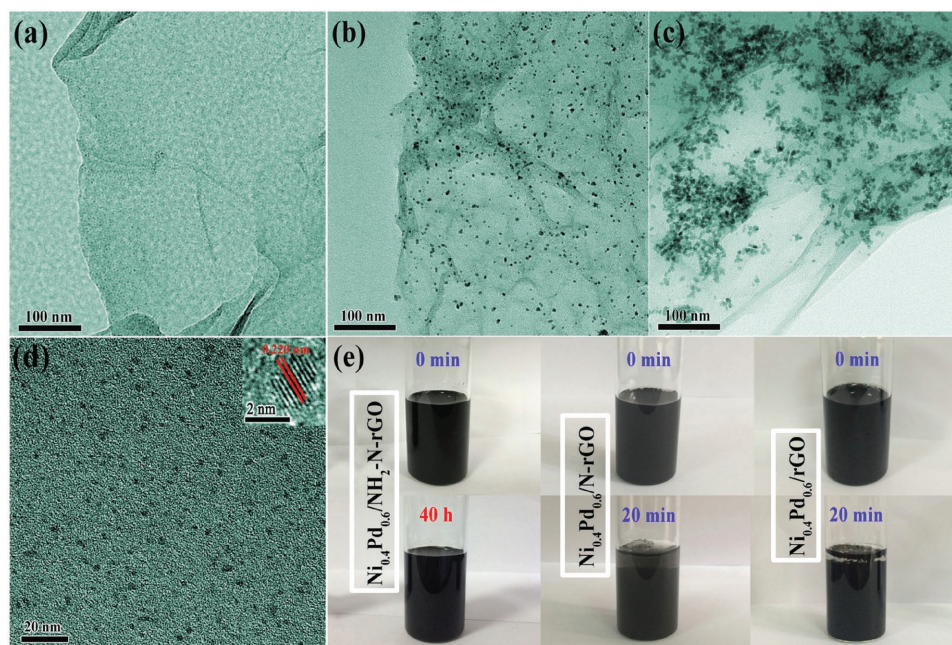


**Figure 1.** TEM images of: a,d)  $\text{Ni}_{0.4}\text{Pd}_{0.6}/\text{NH}_2\text{-N-rGO}$ , b)  $\text{Ni}_{0.4}\text{Pd}_{0.6}/\text{N-rGO}$ , and c)  $\text{Ni}_{0.4}\text{Pd}_{0.6}/\text{rGO}$ ; e) photographs of newly prepared  $\text{Ni}_{0.4}\text{Pd}_{0.6}/\text{NH}_2\text{-N-rGO}$ ,  $\text{Ni}_{0.4}\text{Pd}_{0.6}/\text{N-rGO}$ , and  $\text{Ni}_{0.4}\text{Pd}_{0.6}/\text{rGO}$  specimens, and their corresponding photographs after keeping in aqueous solution for the indicated time.

area, which may lead to the great enhancement in the catalytic activity of  $\text{Ni}_{0.4}\text{Pd}_{0.6}$  active sites (vide infra).

To investigate the detailed crystal and chemical states of the three specimens, X-ray diffraction (XRD), Fourier transform infrared (FTIR) spectroscopy, X-ray photoelectron spectrometry (XPS), and Raman and UV–vis have been applied. **Figure 2a** shows the XRD patterns of the  $\text{Ni}_{0.4}\text{Pd}_{0.6}/\text{NH}_2\text{-N-rGO}$ ,  $\text{Ni}_{0.4}\text{Pd}_{0.6}/\text{N-rGO}$  and  $\text{Ni}_{0.4}\text{Pd}_{0.6}/\text{rGO}$  specimens. It can be seen that the three specimens have the broad C (002) peaks at around  $24.8^\circ$ , which proves the successful reduction of GO to rGO during the preparation process of the specimens,<sup>[13]</sup> and this has also been proved by the Raman, UV–vis, and XPS analyses (Figures S3–S5, Supporting Information).<sup>[7e,13,14]</sup> Besides the diffraction of C (002), the peaks between those of metallic Ni (111) (JCPDS: 65-2865)<sup>[11]</sup> and Pd (111) (JCPDS: 65-2867)<sup>[13]</sup> are also observed for the three specimens from **Figure 2a**, which agrees very well with the HRTEM image of  $\text{Ni}_{0.4}\text{Pd}_{0.6}$  (**Figure 1d**, inset). The XRD and HRTEM results indicate that  $\text{Ni}_{0.4}\text{Pd}_{0.6}$  is formed in an alloy structure, and this can be further confirmed by the XRD pattern of  $\text{Ni}_{0.4}\text{Pd}_{0.6}/\text{NH}_2\text{-N-rGO}$  after heat treatment at 873 K for 3 h in Ar atmosphere (**Figure S6**, Supporting Information), where all the diffraction peaks are located between those of metallic Ni and Pd. **Figure 2b** shows the FTIR of the three specimens. For  $\text{Ni}_{0.4}\text{Pd}_{0.6}/\text{rGO}$ , only a small peak corresponding to aromatic C=C stretching vibration ( $\approx 1544\text{ cm}^{-1}$ ) can be observed,<sup>[15]</sup> namely, there is no other element or group modification on the rGO of this specimen. For  $\text{Ni}_{0.4}\text{Pd}_{0.6}/\text{N-rGO}$ , besides the peaks of C=C and C–OH ( $1402\text{ cm}^{-1}$ ),<sup>[16]</sup> a new band at  $965\text{ cm}^{-1}$  assigned to C–N stretching vibration can also be found,<sup>[17]</sup> which proves that N element has been successfully doped in the rGO of this specimen.<sup>[17]</sup> While for  $\text{Ni}_{0.4}\text{Pd}_{0.6}/\text{NH}_2\text{-N-rGO}$ , except C=C, C–OH, and C–N,<sup>[18a–b]</sup> the appearance of another two bands at 894

and  $1636\text{ cm}^{-1}$ , which could be ascribed to the out of plane and in-plane N–H bending vibrations, respectively,<sup>[18]</sup> confirming the existence of amine (–NH<sub>2</sub>) group on the N-rGO of this specimen. To further confirm the chemical states of N in  $\text{Ni}_{0.4}\text{Pd}_{0.6}/\text{NH}_2\text{-N-rGO}$  and  $\text{Ni}_{0.4}\text{Pd}_{0.6}/\text{N-rGO}$ , the high-resolution XPS analyses have also been applied. As shown in **Figures 2c,d**, the remarkable peaks of N 1s at  $\approx 398.9$  and  $\approx 399.2\text{ eV}$  have been observed for  $\text{Ni}_{0.4}\text{Pd}_{0.6}/\text{NH}_2\text{-N-rGO}$  and  $\text{Ni}_{0.4}\text{Pd}_{0.6}/\text{N-rGO}$ , respectively, suggesting that the element of N has been successfully incorporated into the two products. The little difference of the two N 1s peak positions may result from the different chemical states of N in the two specimens, where the N (**Figure 2c**) in  $\text{Ni}_{0.4}\text{Pd}_{0.6}/\text{NH}_2\text{-N-rGO}$  is similar to the pyridinic N ( $398.7\text{ eV}$ ) and amine N/pyrrolic N ( $399.7\text{ eV}$ ),<sup>[18b,19,20]</sup> while that in  $\text{Ni}_{0.4}\text{Pd}_{0.6}/\text{N-rGO}$  (**Figure 2d**) can be assigned to pyridinic N ( $398.7\text{ eV}$ ) and pyrrolic N ( $399.7\text{ eV}$ )<sup>[20]</sup> which are identified to be the doping N in atomic chain of graphene.<sup>[20]</sup> Both considering the FTIR and XPS results, N in  $\text{Ni}_{0.4}\text{Pd}_{0.6}/\text{N-rGO}$  is proved to be the doping atoms on rGO, and N in  $\text{Ni}_{0.4}\text{Pd}_{0.6}/\text{NH}_2\text{-N-rGO}$  is existed both as the doping atoms to rGO and also in –NH<sub>2</sub> group on surface of rGO, which are schematically shown in **Figures 2e,f**. Therefore, by considering the types of N on rGO, the two specimens are named as  $\text{Ni}_{0.4}\text{Pd}_{0.6}/\text{N-rGO}$  (doping N on rGO) and  $\text{Ni}_{0.4}\text{Pd}_{0.6}/\text{NH}_2\text{-N-rGO}$  (doping N and amine N on rGO), respectively.

To study the electronic effects of Ni to Pd and NH<sub>2</sub>-N-rGO on  $\text{Ni}_{0.4}\text{Pd}_{0.6}$  UPs, XPS analysis has been applied on specimens of the  $\text{Ni}_{0.4}\text{Pd}_{0.6}/\text{NH}_2\text{-N-rGO}$ , Pd/NH<sub>2</sub>-N-rGO, Ni/NH<sub>2</sub>-N-rGO, and free  $\text{Ni}_{0.4}\text{Pd}_{0.6}$ , as shown in **Figure 3**. It can be seen that Pd and Ni in  $\text{Ni}_{0.4}\text{Pd}_{0.6}/\text{NH}_2\text{-N-rGO}$  are mostly in metallic Pd<sup>0</sup> (**Figure 3a**, black trace) and Ni<sup>0</sup> (**Figure 3b**, black trace), respectively<sup>[4b,21]</sup> (a small amount of Ni<sup>II</sup> and Pd<sup>II</sup> can be attributed to the surface oxidation of Pd and Ni during sample

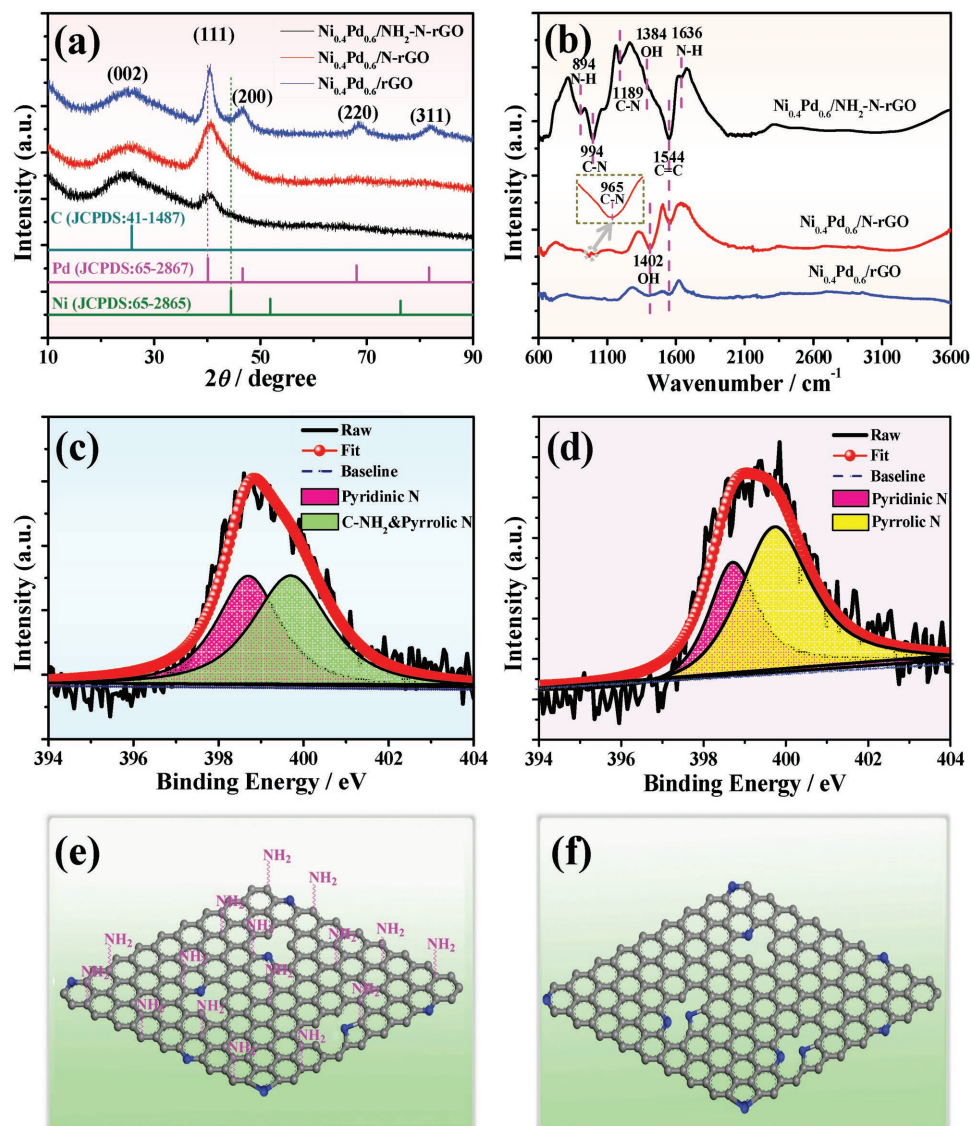


**Figure 2.** a) XRD patterns and b) FTIR spectra of  $\text{Ni}_{0.4}\text{Pd}_{0.6}/\text{NH}_2\text{-N-rGO}$ ,  $\text{Ni}_{0.4}\text{Pd}_{0.6}/\text{N-rGO}$ , and  $\text{Ni}_{0.4}\text{Pd}_{0.6}/\text{rGO}$ ; c,d) high-resolution XPS spectra of Ni 1s in  $\text{Ni}_{0.4}\text{Pd}_{0.6}/\text{NH}_2\text{-N-rGO}$  (c) and  $\text{Ni}_{0.4}\text{Pd}_{0.6}/\text{N-rGO}$  (d); e,f) schematic illustration of  $\text{NH}_2\text{-N-rGO}$  (e) and  $\text{N-rGO}$  (f).

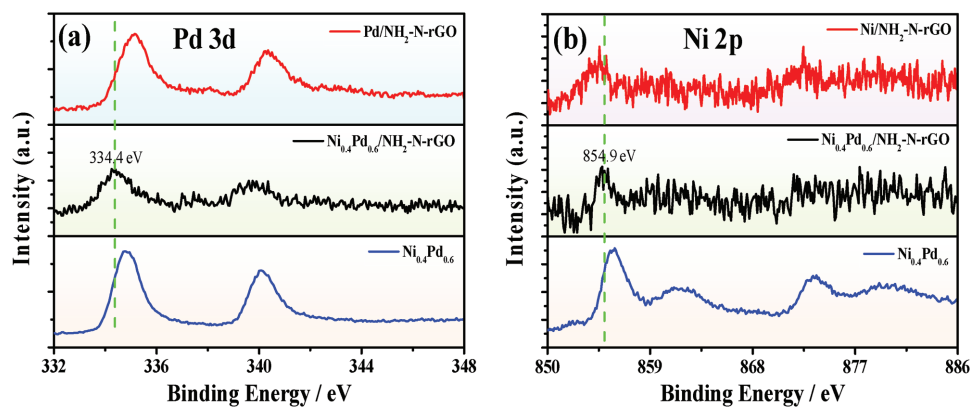


**Figure 3.** High-resolution XPS spectra of: a) Pd 3d and b) Ni 2p in  $\text{Ni}_{0.4}\text{Pd}_{0.6}/\text{NH}_2\text{-N-rGO}$ ,  $\text{Pd}/\text{NH}_2\text{-N-rGO}$ ,  $\text{Ni}/\text{NH}_2\text{-N-rGO}$ , and  $\text{Ni}_{0.4}\text{Pd}_{0.6}$  specimens.

preparing for XPS<sup>[22]</sup>). However, comparing Ni<sub>0.4</sub>Pd<sub>0.6</sub>/NH<sub>2</sub>-N-rGO with Pd/NH<sub>2</sub>-N-rGO, Ni/NH<sub>2</sub>-N-rGO (Figures 3a,b), the Pd 3d peaks are shifted to the lower binding energies, while the Ni 2p peaks are shifted to the higher values. These shifts might be attributed to a partial electron-transfer from Ni to Pd, which can be easily understood by the lower electronegativity of element Ni than Pd (Pd 2.2; Ni 1.8).<sup>[23]</sup> In addition, comparing Ni<sub>0.4</sub>Pd<sub>0.6</sub>/NH<sub>2</sub>-N-rGO with unsupported Ni<sub>0.4</sub>Pd<sub>0.6</sub>, the Pd 3d and Ni 2p peaks are both shifted to the lower binding energies, indicating that some electrons are transferred from the NH<sub>2</sub>-N-rGO substrate to the Ni<sub>0.4</sub>Pd<sub>0.6</sub> UPs, and confirming the strong interaction between the substrate and Ni<sub>0.4</sub>Pd<sub>0.6</sub> UPs. Because the XPS peak intensity is proportional to the concentration (the molar ratio of Ni:Pd is 0.4:0.6 in Ni<sub>0.4</sub>Pd<sub>0.6</sub>/NH<sub>2</sub>-N-rGO) and the sensitivity factors (Ni is 4.044, and Pd is 5.356) of the element on the surface,<sup>[23d]</sup> and hence the peak of Ni is relatively weak in Figure 3. Based on the above XPS analysis, it can be deduced that the addition of Ni to Pd can adjust the electron structure of Pd through the electron synergetic effect, while the support of NH<sub>2</sub>-N-rGO can also modify the electron structure of the

metal UPs through the strong SMSI effect. Through the above two effects, the Pd active sites are electron-rich, which can facilitate to produce H<sub>2</sub> and CO<sub>2</sub> due to the promotion of rate-determining step for the C–H scission in the absorbed HCOO\* intermediate on the catalyst,<sup>[8]</sup> and this has been immediately proved by the following catalytic results.

The catalytic performance of the as-prepared Ni<sub>0.4</sub>Pd<sub>0.6</sub>/NH<sub>2</sub>-N-rGO hybrid together with Ni<sub>0.4</sub>Pd<sub>0.6</sub>/N-rGO, Ni<sub>0.4</sub>Pd<sub>0.6</sub>/rGO, and Ni<sub>0.4</sub>Pd<sub>0.6</sub> nanoparticles prepared with/without APTS (Ni<sub>0.4</sub>Pd<sub>0.6</sub>-APTS and Ni<sub>0.4</sub>Pd<sub>0.6</sub>) for H<sub>2</sub> generation from FA (1.0 M, 5 mL) decomposition at 298 K under ambient atmosphere is shown in Figure 4a for comparison, in order to better observe the effect of APTS and rGO on the catalytic performance. Obviously, Ni<sub>0.4</sub>Pd<sub>0.6</sub>/NH<sub>2</sub>-N-rGO catalyst shows the highest activity among all the prepared catalysts, with which 245 mL of gas can be released in only 4 min, corresponding to a 100% conversion. Considering the actual molar number of the metal is 0.1 mmol ( $n_{\text{metal}} = 0.1 \text{ mmol}$  and metal loading = 20 wt%, which are tested by ICP-AES), the initial turnover frequency (TOF; Equation (S2), Supporting Information)<sup>[9]</sup> is measured to

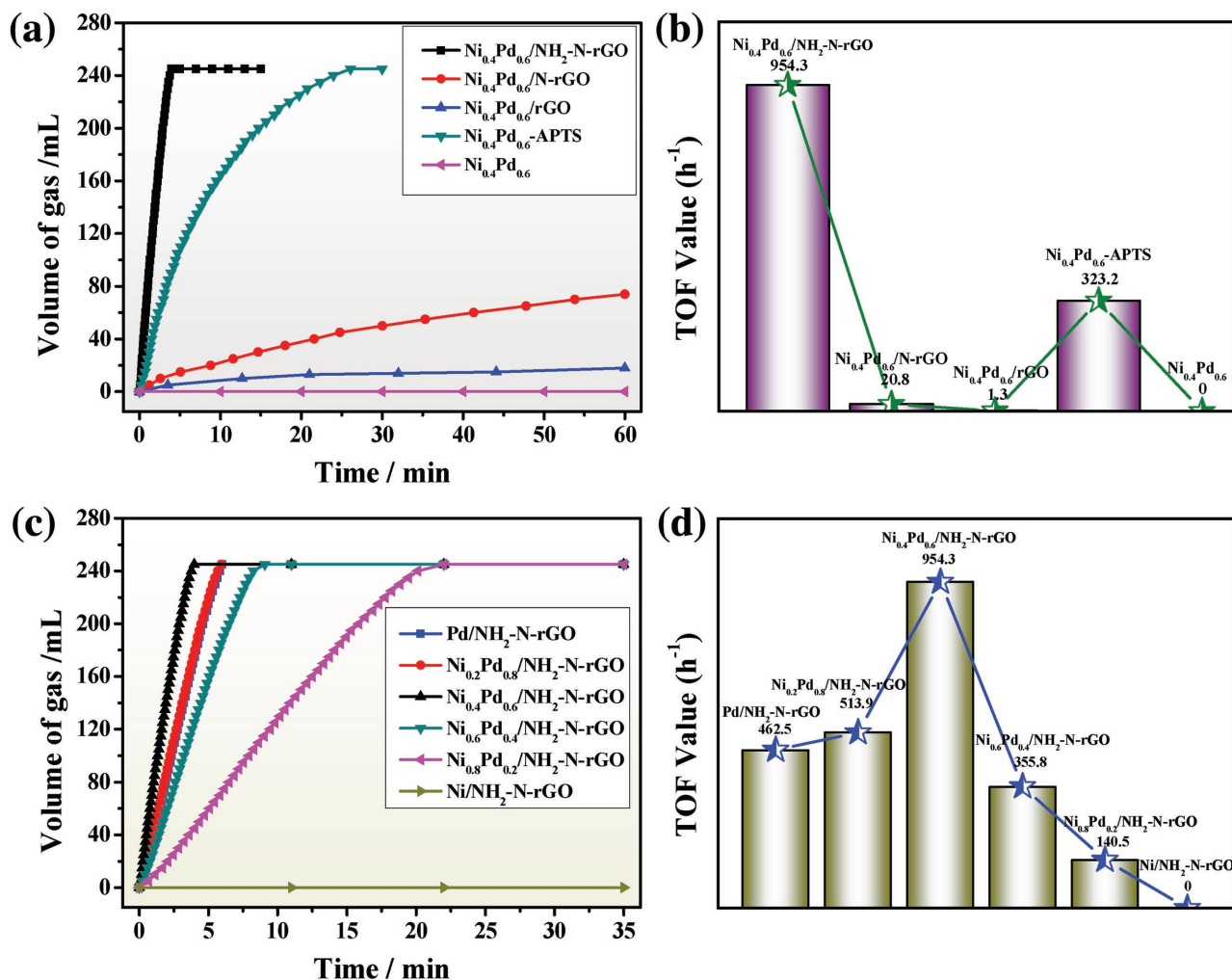


**Figure 4.** a) Gas generation from the decomposition of FA (1.0 M, 5.0 mL) versus time in the presence of Ni<sub>0.4</sub>Pd<sub>0.6</sub> with/without different supports or APTS and b) the corresponding TOF value; c,d) gas generation from the decomposition of FA (1.0 M, 5.0 mL) versus time in the presence of Ni/Pd/NH<sub>2</sub>-N-rGO with different Ni:Pd molar ratios (c) and the corresponding TOF value ( $n_{\text{metal}}/n_{\text{FA}} = 0.02$ ) (d).

be 954.3 mol H<sub>2</sub> mol catalyst<sup>-1</sup> h<sup>-1</sup> without additive at 298 K. As it is known, this value is one of the highest among all the reported heterogeneous catalysts for this reaction without additive (Table S1, Supporting Information)<sup>[1b,2d,5a-d,6b,7e,12a,24]</sup> and even comparable to most of those obtained with additive or/and at elevated temperature.<sup>[4,5e,6a,c,25]</sup> Additionally, with catalyst of Ni<sub>0.4</sub>Pd<sub>0.6</sub>/NH<sub>2</sub>-N-rGO, only the mixture of H<sub>2</sub> and CO<sub>2</sub> but no CO (detection limit: ≈10 ppm for CO; Figure S7, Supporting Information) has been detected by GC (Figure S8, Supporting Information) and MS (Figure S9, Supporting Information) analyses, which means that the present Ni<sub>0.4</sub>Pd<sub>0.6</sub>/NH<sub>2</sub>-N-rGO hybrid has an excellent H<sub>2</sub> selectivity for FA dehydrogenation. On the other hand, for catalyst of Ni<sub>0.4</sub>Pd<sub>0.6</sub>/N-rGO, only 74 mL of gas can be released from FA even after 60 min, giving a conversion of only 30%. And for Ni<sub>0.4</sub>Pd<sub>0.6</sub>/rGO, only 18 mL of gas can be generated in 60 min, with conversion of 7%. Ni<sub>0.4</sub>Pd<sub>0.6</sub>-APTS can release the total 245 mL gas in 26 min, while pure Ni<sub>0.4</sub>Pd<sub>0.6</sub> or APTS (Figure S10, Supporting Information) shows no catalytic activity without gas generation. The better catalytic activity of Ni<sub>0.4</sub>Pd<sub>0.6</sub>-APTS than that of Ni<sub>0.4</sub>Pd<sub>0.6</sub>/rGO may be due to the much smaller particle size and thus more surface active sites of Ni<sub>0.4</sub>Pd<sub>0.6</sub> prepared with APTS (≈1.8 nm; Figure S11, Supporting Information) than those prepared with rGO (≈10.1 nm, Figure 1c), and there is no bond formed between Ni<sub>0.4</sub>Pd<sub>0.6</sub> and APTS (Figure S12, Supporting Information). However, the particle dispersity of Ni<sub>0.4</sub>Pd<sub>0.6</sub>-APTS is not as good as that of Ni<sub>0.4</sub>Pd<sub>0.6</sub>/NH<sub>2</sub>-N-rGO. Therefore, Ni<sub>0.4</sub>Pd<sub>0.6</sub>/NH<sub>2</sub>-N-rGO demonstrates the highest activity among all the specimens. Based on the above results, it can be concluded that the use of NH<sub>2</sub>-N-rGO can significantly improve the catalytic activities of Ni<sub>0.4</sub>Pd<sub>0.6</sub> UPs. Obviously, the significant enhancement on the catalytic performance of Ni<sub>0.4</sub>Pd<sub>0.6</sub>/NH<sub>2</sub>-N-rGO may due to the presence of novel hydrophilic NH<sub>2</sub>-N-rGO support that leads to the ultrafine particle sizes, good dispersion, and strong SMSI effect of alloyed Ni<sub>0.4</sub>Pd<sub>0.6</sub> UPs with plentiful and upgraded active sites. It should be noted that the activity of Ni<sub>0.4</sub>Pd<sub>0.6</sub>/NH<sub>2</sub>-N-rGO almost has no relationship with the dosage of APTS in the range of 0–0.6 mL, while for further increase in the dosage higher than 0.6 mL, the activity will be decreased (Figure S13, Supporting Information).

The recycling stability of the Ni<sub>0.4</sub>Pd<sub>0.6</sub>/NH<sub>2</sub>-N-rGO hybrid is also tested by adding an additional aliquot of FA to the reaction vessel after the completion of the previous run. It can be seen that there is no significant decrease in catalytic activity after the 5<sup>th</sup> run (Figure S14, Supporting Information), and the Ni<sub>0.4</sub>Pd<sub>0.6</sub> particles also demonstrate the similar good dispersion and ultrafine sizes with no obvious sedimentation in the reaction solution (Figure S14 (inset), Supporting Information), indicating the good recycling stability of Ni<sub>0.4</sub>Pd<sub>0.6</sub>/NH<sub>2</sub>-N-rGO catalyst.

Up to now, there have been very few reports on the turnover number (TON; Equation (S3), Supporting Information) of FA decomposition over heterogeneous catalysts, which may be due to the poor long-time stability of those catalysts. As shown in Figure S15 (Supporting Information), the TON over Ni<sub>0.4</sub>Pd<sub>0.6</sub>/NH<sub>2</sub>-N-rGO are calculated to be 334 and 585 within 1 and 3 h, respectively, which are comparable to the values obtained by the noble metal catalysts even with additive (Table S2, Supporting Information),<sup>[5e,24f]</sup> demonstrating the relatively good long-time

stability of Ni<sub>0.4</sub>Pd<sub>0.6</sub>/NH<sub>2</sub>-N-rGO with a large amount of non-noble metal.

More interestingly, with different Ni:Pd molar ratios, the prepared NiPd/NH<sub>2</sub>-N-rGO composite shows the excellent catalytic activity for the dehydrogenation of FA at 298 K, except Ni/NH<sub>2</sub>-rGO. As shown in Figure 4b, monometallic Pd/NH<sub>2</sub>-N-rGO and bimetallic Ni<sub>0.2</sub>Pd<sub>0.8</sub>/NH<sub>2</sub>-N-rGO with low content of Ni have the similar activities, and the reaction can be completed within 6 min with the initial TOF of 462.5 and 513.9 mol H<sub>2</sub> mol catalyst<sup>-1</sup> h<sup>-1</sup>, respectively. When Ni addition comes to 40 at%, the obtained Ni<sub>0.4</sub>Pd<sub>0.6</sub>/NH<sub>2</sub>-N-rGO demonstrates the best activity. Further increase in the Ni content to 60%, the activity of the bimetallic system decreased slightly, with the initial TOF of 355.8 mol H<sub>2</sub> mol catalyst<sup>-1</sup> h<sup>-1</sup>. However, even when the Ni content reaches 80 at%, the resultant Ni<sub>0.8</sub>Pd<sub>0.2</sub>/NH<sub>2</sub>-rGO also shows the excellent activity with full conversion and high initial TOF (140.5 mol H<sub>2</sub> mol catalyst<sup>-1</sup> h<sup>-1</sup>). The actual molar ratios of Ni:Pd in Ni<sub>0.2</sub>Pd<sub>0.8</sub>/NH<sub>2</sub>-N-rGO, Ni<sub>0.6</sub>Pd<sub>0.4</sub>/NH<sub>2</sub>-N-rGO, and Ni<sub>0.8</sub>Pd<sub>0.2</sub>/NH<sub>2</sub>-N-rGO are measured by ICP-AES to be 0.22:0.78, 0.62:0.38, and 0.82:0.18, respectively, which is consistent to nominal molar ratios of Ni:Pd in the samples. To the best of our knowledge, this is the first report on catalyst for hydrogen generation from FA with such a high NNM contents (up to 80 at%) but excellent catalytic activities (Table S1, Supporting Information). Due to the chemical instability and catalytic inactivity of NNM (such as Ni and Co) in FA solution, there is still no report on heterogeneous catalyst with content of NNM higher than 40 at%.<sup>[6]</sup>

To better understand the superiority of the present Ni<sub>0.4</sub>Pd<sub>0.6</sub>/NH<sub>2</sub>-N-rGO catalyst, in situ carbon dioxide infrared spectroscopy (CO-IR) has been applied to determine the surface adsorption properties of Ni<sub>0.4</sub>Pd<sub>0.6</sub>/NH<sub>2</sub>-N-rGO, Ni/NH<sub>2</sub>-N-rGO, and Pd/NH<sub>2</sub>-N-rGO for comparison. As shown in Figure S16 (Supporting Information), intrinsic Ni displays no adsorption to CO. The vibration bands for Pd/NH<sub>2</sub>-N-rGO appeared at 1951 cm<sup>-1</sup>, which can be assigned to bridged CO adsorption.<sup>[26a]</sup> While after the addition of Ni, the bridge-adsorption CO is presented at 1936 cm<sup>-1</sup> for the NiPd/NH<sub>2</sub>-N-rGO catalyst, showing a significant redshift of about 15 cm<sup>-1</sup> when compared to Pd/NH<sub>2</sub>-N-rGO. The redshift is ascribed to that the neighboring Ni atoms could increase the electronic density of Pd and change the surface performance of the catalysts through geometric “ensemble effects” and electronic “ligand effects,”<sup>[26a,b]</sup> which is consistent with the XPS result, and thus enhance the catalytic activity. Moreover, for Ni<sub>0.4</sub>Pd<sub>0.6</sub>/NH<sub>2</sub>-N-rGO, a new linear-bonded CO peak centered at 2059 cm<sup>-1</sup> is appeared, which is caused by the low-coordinated Pd sites in the catalyst, such as corners and defects.<sup>[26c]</sup> Adsorbate is easy to desorb on low-coordinated Pd sites thanks to the relatively low adsorption enthalpy, which may lead to an improvement on the selectivity.<sup>[26d]</sup> Hence, the as-prepared Ni<sub>0.4</sub>Pd<sub>0.6</sub>/NH<sub>2</sub>-N-rGO exhibits the outstanding catalytic activity and 100% H<sub>2</sub> selectivity. Therefore, in this work, the alloy structure of NiPd may facilitate to increase the stability of Ni in the reaction system, and the unique NH<sub>2</sub>-N-rGO support can further help to form plenty of upgraded reactive sites of NiPd UPs on its surface. The above two factors may be responsible for the high efficiency of NiPd/NH<sub>2</sub>-N-rGO for FA selective dehydrogenation even with high Ni content.

In summary, we have developed a facile one-step strategy to simultaneously synthesize NiPd bimetallic UPs growing on a hydrophilic and bifunctional NH<sub>2</sub>-N-rGO substrate at room temperature within 1 min. The novel NH<sub>2</sub>-N-rGO substrate endows the in situ formed NiPd UPs with ultrafine sizes (1.8 nm), high dispersity, good hydrophilicity, and electron-rich active sites, which are the main factors responsible for the excellent catalytic performance of the NiPd/NH<sub>2</sub>-N-rGO system even with high content of Ni (up to 80 at%) for H<sub>2</sub> generation from FA dehydrogenation at 298 K. The resultant hydrophilic Ni<sub>0.4</sub>Pd<sub>0.6</sub>/NH<sub>2</sub>-N-rGO composite exhibits the most excellent activity, good stability, and 100% H<sub>2</sub> selectivity and conversion for FA dehydrogenation, with which the initial TOF can reach the highest value of 954.3 mol H<sub>2</sub> mol catalyst<sup>-1</sup> h<sup>-1</sup> ever reported without any additive at 298 K. The improvement of the NNM-containing NiPd/NH<sub>2</sub>-N-rGO may further promote the practical application of FA as the H<sub>2</sub> storage/generation material. Moreover, the present rapid and facile synthetic method for the preparation of hydrophilic catalyst with ultrafine and good dispersion UPs may expand to some other metallic systems to be applied in reactions in aqueous solution.

## Supporting Information

Supporting Information is available from the Wiley Online Library or from the author.

## Acknowledgements

This work was supported in part by the National Natural Science Foundation of China (Grant Nos. 51522101, 51631004, 51471075, and 51401084) and Program for JLU Science and Technology Innovative Research Team (Grant No. 2017TD-09).

## Conflict of Interest

The authors declare no conflict of interest.

## Keywords

catalysts, formic acid, high efficiency, hydrogen, low cost

Received: May 31, 2017

Revised: August 14, 2017

Published online:

- [1] a) J. A. Turner, *Science* **2004**, 305, 972; b) J. M. Yan, Z. L. Wang, L. Gu, S. J. Li, H. L. Wang, W. T. Zheng, Q. Jiang, *Adv. Energy Mater.* **2015**, 5, 1500107; c) L. Schlögl, A. Züttel, *Nature* **2001**, 414, 353; d) X. Xu, Y. Chen, W. Zhou, Z. Zhu, C. Su, M. Liu, Z. Shao, *Adv. Mater.* **2016**, 28, 6442; e) A. V. Puga, A. Forneli, H. Garcia, A. Corma, *Adv. Funct. Mater.* **2014**, 24, 241.
- [2] a) M. Grasemann, G. Laurenczy, *Energy Environ. Sci.* **2012**, 5, 8171; b) Z. Zheng, T. Tachikawa, T. Majima, *J. Am. Chem. Soc.* **2015**, 137, 948; c) S. Moret, P. J. Dyson, G. Laurenczy, *Nat. Commun.* **2014**, 5, 4017; d) Z. L. Wang, J. M. Yan, Y. Ping, H. L. Wang, W. T. Zheng, Q. Jiang, *Angew. Chem., Int. Ed.* **2013**, 52, 4406.
- [3] a) K. Jiang, K. Xu, S. Zou, W. B. Cai, *J. Am. Chem. Soc.* **2014**, 136, 4861; b) X. Yang, P. Pachfule, Y. Chen, N. Tsumori, Q. Xu, *Chem. Commun.* **2016**, 52, 4171; c) Y. Ping, J. M. Yan, Z. L. Wang, H. L. Wang, Q. Jiang, *J. Mater. Chem. A* **2013**, 1, 12188; d) J. Cheng, X. Gu, X. Sheng, P. Liu, H. Su, *J. Mater. Chem. A* **2016**, 4, 1887; e) W. Y. Yu, G. M. Mullen, D. W. Flaherty, C. B. Mullins, *J. Am. Chem. Soc.* **2014**, 136, 11070.
- [4] a) Z. L. Wang, J. M. Yan, H. L. Wang, Y. Ping, Q. Jiang, *Sci. Rep.* **2012**, 2, 598; b) M. Yurderi, A. Bulut, M. Zahmakiran, M. Kaya, *Appl. Catal., B* **2014**, 160–161, 514.
- [5] a) J. H. Lee, J. Ryu, J. Y. Kim, S. W. Nam, J. H. Han, T. H. Lim, S. Gautam, K. H. Chae, C. W. Yoon, *J. Mater. Chem. A* **2014**, 2, 9490; b) S. Zhang, O. Metin, D. Su, S. Sun, *Angew. Chem., Int. Ed.* **2013**, 52, 3681; c) O. Metin, X. Sun, S. Sun, *Nanoscale* **2013**, 5, 910; d) C. Hu, S. W. Ting, J. Tsui, K. Y. Chan, *Int. J. Hydrogen Energy* **2012**, 37, 6372; e) Q. Y. Bi, X. L. Du, Y. M. Liu, Y. Cao, H. Y. He, K. N. Fan, *J. Am. Chem. Soc.* **2012**, 134, 8926.
- [6] a) Y. Chen, Q. L. Zhu, N. Tsumori, Q. Xu, *J. Am. Chem. Soc.* **2015**, 137, 106; b) Z. L. Wang, Y. Ping, J. M. Yan, H. L. Wang, Q. Jiang, *Int. J. Hydrogen Energy* **2014**, 39, 4850; c) Y. L. Qin, J. Wang, F. Z. Meng, L. M. Wang, X. B. Zhang, *Chem. Commun.* **2013**, 49, 10028; d) L. Yang, W. Luo, G. Cheng, *Int. J. Hydrogen Energy* **2016**, 41, 439; e) Y. Qin, X. Zhang, X. Dai, H. Sun, Y. Yang, X. Li, Q. Shi, D. Gao, H. Wang, N. F. Yu, S. G. Sun, *Small* **2016**, 12, 524.
- [7] a) C. Ma, W. Xue, J. Li, W. Xing, Z. Hao, *Green Chem.* **2013**, 15, 1035; b) T. T. Zhang, H. Y. Zhao, S. N. He, K. Liu, H. Y. Liu, Y. D. Yin, C. B. Gao, *ACS Nano* **2014**, 8, 7297; c) H. Wang, T. Maiyalagan, X. Wang, *ACS Catal.* **2012**, 2, 781; d) M. Liu, Y. Lu, W. Chen, *Adv. Funct. Mater.* **2013**, 23, 1289; e) Z. L. Wang, J. M. Yan, H. L. Wang, Y. Ping, Q. Jiang, *J. Mater. Chem. A* **2013**, 1, 12721.
- [8] a) K. Tedsree, C. W. A. Chan, S. Jones, Q. Cuan, W. K. Li, X. Q. Gong, S. C. E. Tsang, *Science* **2011**, 332, 224; b) K. Mori, M. Dojo, H. Yamashita, *ACS Catal.* **2013**, 3, 1114; c) M. Ojeda, E. Iglesia, *Angew. Chem., Int. Ed.* **2009**, 48, 4800; d) B. Dehghanzad, M. K. R. Aghjeh, O. Rafeie, A. Tavakoli, A. J. Oskoorie, *RSC Adv.* **2016**, 6, 3578; e) A. Chakravarty, K. Bhowmik, A. Mukherjee, G. De, *Langmuir* **2015**, 31, 5210; f) M. Zhang, Y. Li, Z. Yan, J. Jing, J. Xie, M. Chen, *Electrochim. Acta* **2015**, 158, 81.
- [9] See Supporting Information.
- [10] S. M. Hong, S. H. Kim, K. B. Lee, *Energy Fuels* **2013**, 27, 3358.
- [11] D. Wang, Y. Li, *J. Am. Chem. Soc.* **2010**, 132, 6280.
- [12] a) Z. L. Wang, H. L. Wang, J. M. Yan, Y. Ping, S. I. O, S. J. Li, Q. Jiang, *Chem. Commun.* **2014**, 50, 2732; b) S. Gao, W. Liu, C. Feng, N. Z. Shang, C. Wang, *Catal. Sci. Technol.* **2016**, 6, 869.
- [13] S. J. Li, Y. Ping, J. M. Yan, H. L. Wang, M. Wu, Q. Jiang, *J. Mater. Chem. A* **2015**, 3, 14535.
- [14] a) Z. L. Wang, J. M. Yan, Y. F. Zhang, Y. Ping, H. L. Wang, Q. Jiang, *Nanoscale* **2014**, 6, 3073; b) S. Thakur, N. Karak, *Carbon* **2012**, 50, 5331; c) M. Latorre-Sanchez, A. Primo, H. Garcia, *Angew. Chem., Int. Ed.* **2013**, 52, 11813.
- [15] S. Sandoval, N. Kumar, J. O. Sole, A. Sundaresan, C. N. R. Rao, A. Fuertes, G. Tobias, *Carbon* **2016**, 96, 594.
- [16] a) S. Wang, J. Li, X. Zhou, C. Zheng, J. Ning, Y. Zhong, Y. Hu, *J. Mater. Chem. A* **2014**, 2, 19815; b) M. S. A. S. Shah, W. J. Kim, J. Park, D. K. Rhee, I. H. Jang, N. G. Park, J. Y. Lee, P. J. Yoo, *ACS Appl. Mater. Interface* **2014**, 6, 20819.
- [17] Z. Lin, M. Song, Y. Ding, Y. Liu, M. Liu, C. Wong, *Phys. Chem. Chem. Phys.* **2012**, 14, 3381.
- [18] a) S. K. Singh, M. K. Singh, P. P. Kulkarni, V. K. Sonkar, J. A. Gracio, D. Dash, *ACS Nano* **2012**, 6, 2731; b) L. Lai, L. Chen, D. Zhan, L. Sun, J. Liu, S. H. Lim, C. K. Poh, Z. Shen, J. Lin, *Carbon* **2011**, 49, 3250; c) A. Chakravarty, D. Sengupta, B. Basu, A. Mukherjee, G. De, *RSC Adv.* **2015**, 5, 92585; d) A. Chakravarty, K. Bhowmik, G. De, A. Mukherjee, *New J. Chem.* **2015**, 39, 2451; e) T. Ramanathan, F. T. Fisher, R. S. Ruoff, L. C. Brinson, *Chem. Mater.* **2015**, 17, 1290.

- [19] W. Ye, Y. Chen, Y. Zhou, J. Fu, W. Wu, D. Gao, F. Zhou, C. Wang, D. Xue, *Electrochim. Acta* **2014**, *142*, 18.
- [20] a) L. Jia, D. A. Bulushev, O. Y. Podyacheva, A. I. Boronin, L. S. Kibis, E. Y. Gerasimov, S. Beloshapkin, I. A. Seryak, Z. R. Ismagilov, J. R. H. Ross, *J. Catal.* **2013**, *307*, 94; b) S. Liu, J. Xie, H. Li, Y. Wang, H. Y. Yang, T. Zhu, S. Zhang, G. Cao, X. Zhao, *J. Mater. Chem. A* **2014**, *2*, 18125; c) S. Indrawirawan, H. Sun, X. Duan, S. Wang, *J. Mater. Chem. A* **2015**, *3*, 3432; d) D. Deng, X. Pan, L. Yu, Y. Cui, Y. Jiang, J. Qi, W. X. Li, Q. Fu, X. Ma, Q. Xue, G. Sun, X. Bao, *Chem. Mater.* **2011**, *23*, 1188.
- [21] A. R. Naghash, T. H. Etsell, S. Xu, *Chem. Mater.* **2006**, *18*, 2480.
- [22] a) T. Pillo, R. Zimmermann, P. Steiner, S. Hufner, *J. Phys: Condens. Matter.* **1997**, *9*, 3987; b) M. S. Hamdan, Riyanto, M. R. Othman, *Int. J. Electrochem. Sci.* **2013**, *8*, 4747; c) M. Zhao, K. Abe, S. Yamaura, Y. Yamamoto, N. Asao, *Chem. Mater.* **2014**, *26*, 1056.
- [23] a) C. Zhu, D. Wen, M. Oschatz, M. Holzschuh, W. Liu, A. K. Herrmann, F. Simon, S. Kaskel, A. Eychmuller, *Small* **2015**, *11*, 1430; b) R. Li, Z. Wei, T. Huang, A. Yu, *Electrochim. Acta* **2011**, *56*, 6860; c) U. B. Demirci, *J. Power Sources* **2007**, *173*, 11; d) C. D. Wagner, L. E. Davis, M. V. Zeller, J. A. Taylor, R. H. Raymond, L. H. Gale, *Surf. Interface Anal.* **1981**, *3*, 211.
- [24] a) Y. Karatas, A. Bulut, M. Yurderi, I. E. Ertas, O. Alal, M. Gulcan, M. Celebi, H. Kivrak, M. Kaya, M. Zahmakiran, *Appl. Catal., B* **2016**, *180*, 586; b) S. Jones, J. Qu, K. Tedsree, X. Q. Gong, S. C. E. Tsang, *Angew. Chem., Int. Ed.* **2012**, *51*, 11275; c) A. Bulut, M. Yurderi, Y. Karatas, M. Zahmakiran, H. Kivrak, M. Gulcan, M. Kaya, *Appl. Catal., B* **2015**, *164*, 324; d) K. Tedsree, T. Li, S. Jones, C. W. A. Chan, K. M. K. Yu, P. A. J. Bagot, E. A. Marquis, G. D. W. Smith, S. C. E. Tsang, *Nat. Nanotechnol.* **2011**, *6*, 302; e) Y. Y. Cai, X. H. Li, Y. N. Zhang, X. Wei, K. X. Wang, J. S. Chen, *Angew. Chem., Int. Ed.* **2013**, *125*, 12038; f) Q. Y. Bi, J. D. Lin, Y. M. Liu, H. Y. He, F. Q. Huang, Y. Cao, *Angew. Chem., Int. Ed.* **2016**, *55*, 11849.
- [25] a) X. Gu, Z. H. Lu, H. L. Jiang, T. Akita, Q. Xu, *J. Am. Chem. Soc.* **2011**, *133*, 11822. b) S. Wu, F. Yang, H. Wang, R. Chen, P. Sun, T. Chen, *Chem. Commun.* **2015**, *51*, 10887; c) Q. L. Zhu, N. Tsumori, Q. Xu, *Chem. Sci.* **2014**, *5*, 195.
- [26] a) S. Su, W. Lin, H. Cheng, C. Zhang, Y. Li, T. Liu, B. Zhang, Q. Wu, X. Yu, F. Zhao, *RSC Adv.* **2016**, *6*, 103650; b) A. Haghofer, K. Fottinger, F. Girgsdies, D. Teschner, A. K. Gericke, R. Schlogl, G. Rupprechter, *J. Catal.* **2012**, *286*, 13; c) M. Li, D. Weng, X. Wu, J. Wan, B. Wang, *Catal. Today* **2013**, *201*, 19; d) Y. He, J. Fan, J. Feng, C. Luo, P. Yang, D. Li, *J. Catal.* **2015**, *331*, 118.